Acoustic Birefringence Changes in the Base Metal and Heat Affected Zone of ASTM 1020 Steel under Plastic Deformation and Fatigue

Alexander Gonchar*, *Vyacheslav* Klyushnikov, and *Vasily* Mishakin

Institute of Applied Physics of the RAS, Nizhny Novgorod, Russia

Abstract. This paper deals with metallographic studies and ultrasonic investigations of acoustic birefringence in the base metal and heat affected zone of welded specimens of ASTM 1020 steel under uniaxial tension and low-cycle fatigue. We examined microstructural changes on the surface using optical microscope. It was found that development of slip bands differs in the base metal and heat affected zone. The ultrasonic pulse echo method was used for the determination of acoustic birefringence and velocities of ultrasonic shear waves. The differences in the change in velocities in the base metal and in heat affected zone were revealed. Acoustic birefringence was found to change monotonously in the base metal under fatigue as well as in the base metal and heat affected zone under uniaxial tension. For heat affected zone, during fatigue, acoustic birefringence was found to change non-monotonously up to cycle ratio of 0.3 and decrease monotonously after cycle ratio of 0.3. Based on the relationship between relative number of loading cycles, or plasticity resource, and acoustic birefringence, ultrasonic techniques were proposed for assessing damage.

Introduction

Fatigue failure prediction and residual strain estimation are a common scientific and technical challenge. To define relationships between microstructure-sensitive parameters and material response to damage, it is available to use engineering techniques of non-destructive testing. The acoustic birefringence technique is widely used for assessing damage and monitoring the material state [1-6]. This technique has several advantages: it is applicable for industrial use due to its simplicity and reliability; there is no need to know the thickness of the structural element; noncontact electromagnetic acoustic transducers can be used; acoustic birefringence is independent of temperature [7-9].

The production of metal structures often involves welding. Fatigue failure of welded joints is one of the most dangerous damage for welded structures [10-12]. During welding, the weld and the adjacent area are heated up to Ac3 temperature. In the heat affected zone (HAZ), the metal is characterized by a reduced yield stress in comparison with the base

* Corresponding author: avg-ndt@mail.ru

© The Authors, published by EDP Sciences. This is an open access article distributed under the terms of the Creative Commons Attribution License 4.0 (https://creativecommons.org/licenses/by/4.0/).

metal. The studies of the mechanical properties of welded joints show that HAZ is the most vulnerable area [13-16]. Inhomogeneity of microstructure and mechanical properties of HAZ makes it difficult to monitor the material state.

It is well known that micro defects can form both on the surface and inside the material. Surface and internal microstructural damage may accumulate at different rates, so it is desirable to monitor both of them. To evaluate surface microstructural damage, it is appropriate to use optical method. An important advantage of the optical method is the ability to directly observe microstructure changes on the surface.

In this paper, the base metal and HAZ of low-carbon steel welded joint, subjected to low-cycle fatigue, are investigated using ultrasonic pulse echo method.

Experimental technique

Material. The investigated material was hot-rolled low-carbon ASTM 1020 steel for load-bearing elements of welded and non-welded structures and parts. This steel is widely used for various industrial applications. Chemical composition, determined by an Oxford Instruments Foundry master optical emission spectrometer, was as follows (wt %): 0.18 C, 0.2 Si, 0.65 Mn, < 0.01 S, < 0.02 P, balance Fe. Typical mechanical properties are: yield strength 205÷255 MPa, tensile strength 370÷490 MPa, ultimate elongation (%) 22÷26. Specimens were cut from the base metal and HAZ (incomplete recrystallization zone) of welded joint.

Mechanical tests. Uniaxial tension and low-cycle fatigue tests were performed on the circular cross-section specimens. Geometry and dimensions of the specimens are shown in Fig. 1. Two plane-parallel platforms 10×3 mm in size were cut out to enable ultrasonic measurements and metallographic investigations. A BISS Nano UT 01 0025 servo-hydraulic testing machine was used. Uniaxial tension was carried out step-by-step at a strain rate of 10^{-3} s^{-1}. Each specimen was tested until fracture. Cyclic tension-compression loading conditions were as follows: strain-controlled mode with a strain ratio R = -1; loading frequency of 1 Hz. Specimens were tested step-by-step with strain amplitude of 0.3%. Each specimen was cycled until initiation of a major crack with a length of about 1 mm.

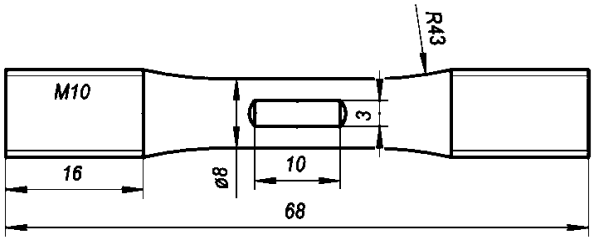

Fig.1. Geometry and dimensions (mm) of specimen.

For each experimental step, after interrupting the test and unloading the specimen ultrasonic measurements and microstructure photographing were carried out. Ambient temperature was 23°C.

Metallographic studies. Before loading, an area for metallographic investigations 10×3 mm in size was prepared in each specimen. Surface was first mechanically polished and then chemical etched using a 5% nitric acid alcohol solution to reveal the grain boundaries. Microstructure of the stress-free specimens was observed using an Altami MET 3M optical microscope. For each specimens, several sets of optical images were obtained by photographing the same area before the test and after each step of the test. For investigated steel, microstructure evolution due to uniaxial tension and low-cycle fatigue mainly consists in the appearance and subsequent growth of persistent slip bands. Metallographic studies have been discussed in detail elsewhere [17].

Ultrasonic measurements. Times-of-flight of two shear waves propagating in the specimen between two plane-parallel platforms and polarized in the mutually perpendicular directions along (t_1) and across (t_2) the loading axis were measured by the pulse echo

method. The shear wave was excited and received by a piezoelectric transducer V157 Olympus, having element 3.2 mm in size with frequency of 5 MHz. It was installed on the plane-parallel platform in the gauge section of the specimen. An ultrasonic flaw detector A1212 MASTER ACS was employed as a generator of electrical pulses. A digital oscilloscope LA-n1USB with ADCLab software was used to record an amplitude-time diagram of echo pulses from the piezoelectric transducer on a PC. Sampling frequency was 1 GHz, time resolution was 1 ns. The time-of-flight of the ultrasonic wave was measured between the first and second echo pulses.

Velocities of two orthogonally polarized shear waves were obtained from the ratio of samle thickness *h* to the corresponding times-of-flight

$$V_1 = 2\ h / t_1,\ V_2 = 2\ h / t_2, \quad (1)$$

where V_1 and V_2 – waves propagation velocities polarized along and across the loading axis, respectively; sample thickness was measured by a micrometer.

Next, acoustic birefringence was defined in terms of times-of-flight of two orthogonally polarized shear waves as

$$B = 2\ (t_2 - t_1) / (t_1 + t_2). \quad (2)$$

Change in acoustic birefringence ΔB was calculated as the difference between the subsequent value and initial one. The procedure of ultrasonic measurements was the same as elsewhere [17].

Results

Microstructural change. Fig. 2a and 3a show microstructure of base metal in the initial state. Microstructure of investigated steel is homogeneous and consists of ferrite and perlite grains. The average grain size is 37 μm, and the ferrite/perlite ratio is 90/10. It follows from observations that persistent slip bands appear in the ferrite grains already at the first step of uniaxial tension and of the fatigue test; during further loading, more and more slip bands appear (Fig. 2b and 3b), the dimensions of the already formed slip bands increase, and some slip bands merge, Fig. 2c and 3c.

Fig. 2d and 3d show microstructure of HAZ in the initial state. Microstructure corresponds to incomplete recrystallization of steel. It is characterized by mixed structure consisted of large grains, which have not undergone recrystallization, and clusters of recrystallized small grains. Like as for the base metal, persistent slip bands are formed in the ferrite grains, Fig. 2e, 2f, 3e, 3f.

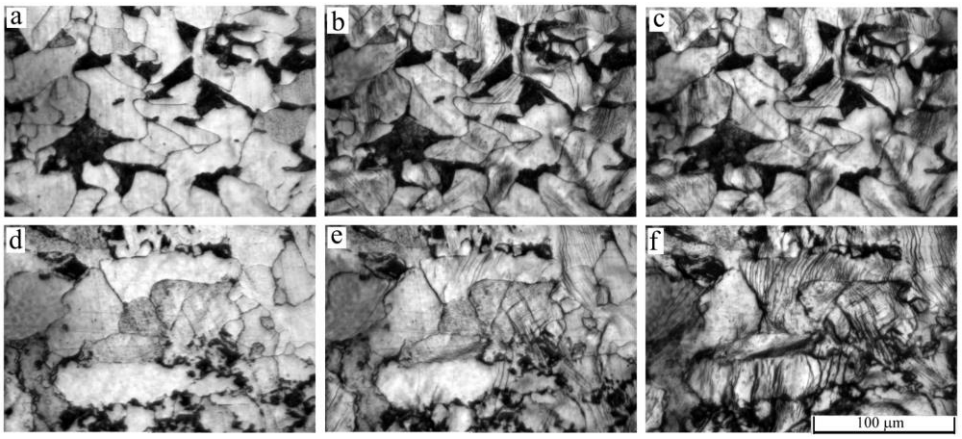

Fig. 2. Photo of microstructure (uniaxial tension): a – initial state of base metal; b – base metal, residual strain ε=15%; c – base metal, ultimate strain ε_f=35%; d – initial state of HAZ; e – HAZ, residual strain ε=17%; f – HAZ, ultimate strain ε_f=38%).

Qualitative analysis of large number of microstructure images showed that the persistent slip bands are formed more actively in HAZ. It should be noted that the ultimate elongation was 38% for HAZ and 35% for the base metal. This fact can be explained by a more active movement of dislocations in the HAZ that produce more intensive formation of persistent slip bands. This is confirmed by microstructural investigation.

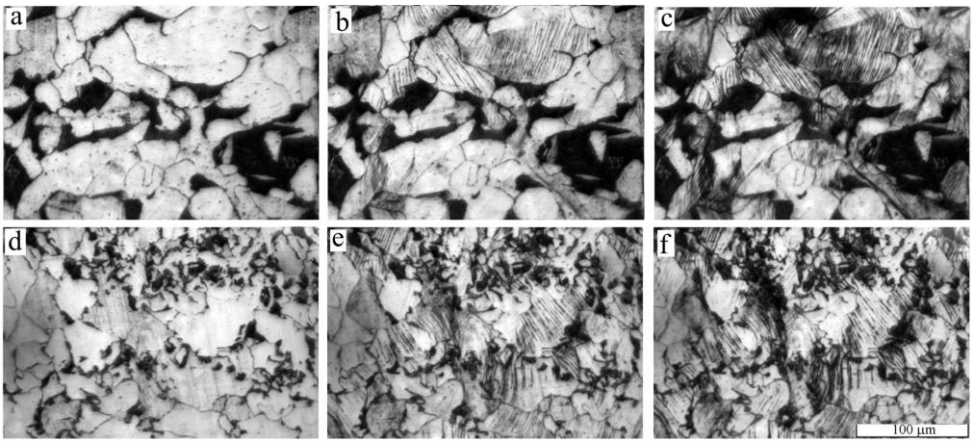

Fig. 3. Photo of microstructure (fatigue): a – initial state of base metal; b – base metal under cyclic loading (N=1000, N/N_f =0.3); c – base metal under cyclic loading (N=3300, N/N_f =1); d – initial state of HAZ; e – HAZ under cyclic loading (N=2000, N/N_f =0.3); f – HAZ under cyclic loading (N=6500, N/N_f =1).

It should also be noted that, at the same strain amplitude, the fatigue life was N_f = 6500 cycles for the HAZ and N_f = 3300 for the base metal. This can be explained by the fact that more active movements of dislocations increase the cyclic durability due to stress relaxation. If the dislocation movement is blocked, then the input energy is spent to the formation of microdefects.

Acoustic birefringence measurements. From ultrasonic investigations of the specimens tested for uniaxial tension in steps the dependences changes of shear wave velocities V_1 and V_2 for the base metal (BM) and for the HAZ on the plastic strain ε, Fig.

4a. There are differences in the behaviour of velocities changes in BM and in the HAZ. It was found that acoustic birefringence increases monotonically with increasing plastic strain, Fig. 4b.

Note that the Fig. 4a shows the dependences for strain less than 17%, while ultimate elongation in percent (ε_f) for HAZ 38% and base metal 35%. It is less than half of the plasticity resource $\varepsilon/\varepsilon_f$. Further deformation ($\varepsilon/\varepsilon_f$ more than 50%) leads to formation an "orange peel" and neck, that breaks the acoustic contact between transducer and surface of specimen. The rate of change in acoustic birefringence for HAZ is higher than for base metal, Fig. 4b.

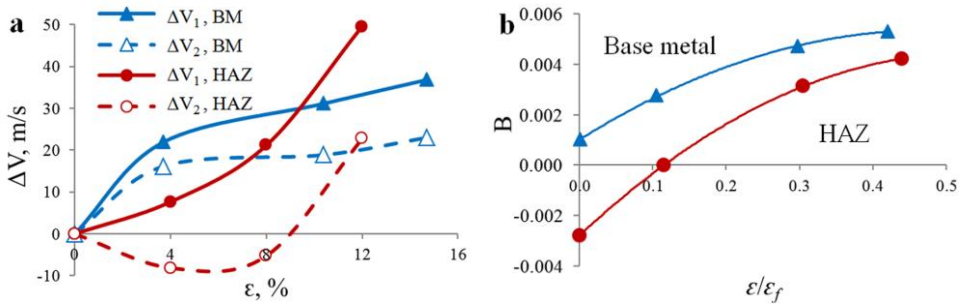

Fig. 4. Dependence of the: a – change of shear wave velocity on the plastic strain; b – acoustic birefringence change on the resource plasticity.

The change of acoustic birefringence for HAZ had approximately one-half higher once for base metal at $\varepsilon/\varepsilon_f = 37\%$ (the last reliably measured point).

Then the plasticity resource can be calculated using the acoustic birefringence change as follows:

$$\varepsilon/\varepsilon_f = k_1 \Delta B^2 + k_2 \Delta B, \quad (3)$$

where k_1=5466, k_2=23 for HAZ and k_1=15585, k_2=28 for base metal.

This relationship can be used for prediction of resource plasticity from ultrasonic data.

From ultrasonic investigations of the specimens tested for fatigue in stages, the dependences changes of shear wave velocities V_1 and V_2 for the base metal (BM) and for the HAZ on the number of loading cycles N, Fig. 5a. For base metal velocities decrease monotonically, for HAZ velocities first increases, then decrease monotonically. The rate of change of velocity and maximum decrease for base metal is higher than for HAZ. The acoustic birefringence for base metal decreases linearly during fatigue loading, Fig. 5b. For HAZ, acoustic birefringence first decreases drastically, then increases drastically, and after 3000 cycles (cycle ratio $N/N_f = 0.3$) decreases linearly. The non-monotonous change in acoustic birefringence can be explained by the relaxation of residual welding stresses. This issue requires in-depth research and is not a subject of this work.

Changes in acoustic birefringence were found to linearly depend on the number of cycles (for HAZ N/N_f from 0.3 to 1), Fig. 5b.

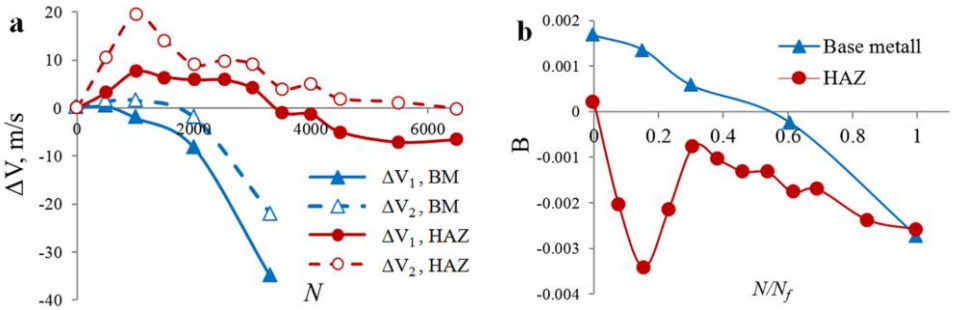

Fig. 5. Dependence of the: a – change of velocity on the number of cycle; b – acoustic birefringence change on the cycle ratio.

The maximum decrease in acoustic birefringence was found to be the same (- 0.0029) for both loading conditions, taking into account the measurement accuracy. In addition, it should be noted that the specimens were heterogeneous in the initial state. As shown in Fig. 5b, in coordinates $\{N/N_f; \Delta B\}$, experimental data for both loading conditions can be represented by a single linear relationship:

$$N/N_f = -348\Delta B. \quad (4)$$

This relationship can be used for prediction of fatigue life from ultrasonic data.

Finally, note that the proposed techniques (Eq.3 and Eq.4) have potential for industrial application.

Conclusion

The evolution of microstructure and the changes in acoustic birefringence under uniaxial tension and low-cycle fatigue in the base metal and HAZ of hot-rolled low-carbon steel were experimentally investigated. The study of microstructure images has shown that the persistent slip bands develops more actively in HAZ that can be explained by more active movement of dislocations. There are differences in the behaviour of velocities changes in BM and in the HAZ under uniaxial tension. For base metal velocities decrease monotonically, for HAZ velocities first increases, then decrease monotonically under fatigue. The rate of change of velocity and maximum decrease for base metal is higher than for HAZ. Acoustic birefringence increases monotonically with strain under uniaxial tension. The rate of change in acoustic birefringence for HAZ is higher than for base metal. Acoustic birefringence was found to decrease linearly with loading cycles under fatigue. The decrease in absolute value of acoustic birefringence due to fatigue is lower than its increase due to uniaxial tension. The results of ultrasonic studies can be used for assessing fatigue damage and plasticity resource of hot-rolled low-carbon ASTM 1020 steel.

This work was supported by the Russian Science Foundation, grant number 21-79-10395.

References

1. L. Carvajal, A. Artigas, A. Monsalve, Y. Vargas, Acoustic birefringence and Poisson's ratio determined by ultrasound: tools to follow-up deformation by cold rolling and recrystallization, Mat. Res. 20 (2017) 1-7.

2. M. Hirao, Y.-H. Pao, Dependence of acoustoelastic birefringence on plastic strains in a beam, J. Acous. Soc. Am. 77 (5) (1985) 1659-1664.

3. A. Belyaev, V. Polyanskiy, A. Semenov, D. Tretyakov, Y. Yakovlev, Investigation of the correlation between acoustic anisotropy, damage and measures of the stress-strain state, Procedia Struct. Integr. 6 (2017) 201–207.

4. S. Gupta, A. Ray, E. Keller, Online fatigue damage monitoring by ultrasonic measurements: A symbolic dynamics approach, Int. J. Fat. 29 (2007) 1100–1114.

5. A. Belyaev, A. Lobachev, A. Modestov, A. Pivkov, V. Polyanskii, A. Semenov, D. Tret'yakov, L. Shtukin, Estimating the plastic strain with the use of acoustic anisotropy, Mech. Solids 51 (2016) 606–611.

6. V. Mishakin, A. Gonchar, K. Kurashkin, V. Klyushnikov, M. Kachanov, On low-cycle fatigue of austenitic steel. Part I: Changes of Poisson's ratio and elastic anisotropy, Int. J. Eng. Sci. 168 (2021) 103567. https://doi.org/10.1016/j.ijengsci.2021.103567

7. K. Makowska, L. Piotrowski, Z. Kowalewski, Prediction of the Mechanical Properties of P91 Steel by Means of Magneto-acoustic Emission and Acoustic Birefringence, J. Nondestruct. Eval. 36 (2017) 43.

8. K. Kurashkin, A. Gonchar, Variation of acoustic characteristics of an aluminum alloy during plastic deformation at room and subzero temperatures, AIP Conf. Proc. (2018) 030030.

9. P. Strážovec, A. Suchánek, P. Šťastniak, J. Harušinec, Detection of residual stress in a railway wheel, Transportation Research Procedia, 40 (2019) 898-905.

10. C. He, C. Huang, Y. Liu, Q. Wang, Fatigue damage evaluation of low-alloy steel welded joints in fusion zone and heat affected zone based on frequency response changes in gigacycle fatigue, Int. J. Fatigue 61 (2014) 297–303.

11. W. Fricke, Fatigue analysis of welded joints: state of development, Mar Struct. 16 (3) (2003) 185-200.

12. M. Toyosada, K. Gotoh, T. Niwa, Fatigue life assessment for welded structures without initial defects: an algorithm for predicting fatigue crack growth from a sound site, Int. J. Fatigue 26 (2004) 993-1002.

13. A. Güral, B. Bostan, A. Özdemir, Heat treatment in two phase region and its effect on welding of a low carbon steel, Mater. Design 28 (2007) 897-903.

14. F. Dittrich, J. Kaars, B. Masek, S. Jenicek, M.V.–X. Wagner, P. Mayr, HAZ characterization of welded 42SiCr steel treated by quenching and partitioning, J. M. Process. Tech. 268 (2019) 37-46.

15. J. Veerababu, S. Goyal, A. Nagesha, Studies on creep-fatigue interaction behavior of Grade 92 steel and its weld joints, Int. J. Fatigue 149 (2021) 106307.

16. L. Lan, G. Shao, Morphological evolution of HAZ microstructures in low carbon steel during simulated welding thermal cycle, Micron 131 (2020) 102828.

17. A. Gonchar, K. Kurashkin, O. Andreeva, M. Anosov, V. Klyushnikov, Fatigue life prediction of structural steel using acoustic birefringence and characteristics of persistent slip bands, Fatigue Fract. Eng. Mater. Struct. 45 (2022) 101-112.